Adiabatic self-heating determination for Ti6Al4V at different temperatures

A. Sela[a,*], G. Ortiz-de-Zarate[a], D. Soler[a], G. Germain[b], L. Gallegos[b], P.J. Arrazola[a]

[a] Faculty of Engineering, Mondragon Unibertsitatea, Arrasate 20500, Spain
[b] Arts et Métiers Campus d'Angers, LAMPA EA1427, 2 bd du Ronceray, Angers 49000, France

Keywords:
Adiabatic self-heating
Infrared measurement
Thermodynamic analysis
Ti6Al4V
Compression test

A B S T R A C T

Nowadays, numerical models are one of the most widely used techniques to predict material performance subjected to different manufacturing processes. However, to obtain accurate predictions, these models require reliable input data from thermomechanical tests. Nevertheless, during the test performance the material is self-heated due to a phenomenon known as adiabatic self-heating. Despite the proven relevance of a proper characterization, adiabatic self-heating is not properly taken into account during thermomechanical tests. In addition, in the literature, two different definitions were found under the umbrella of adiabatic-self heating. On the one hand, it could be defined as the ratio between the heat spent to heat the sample to the plastic work, value commonly taken as 0.9. On the other hand, many authors define the adiabatic heating as the ratio between the heat experimentally measured to the total plastic work. This second approach, although seems easier, is neglecting heat losses. These two different approaches could lead to misunderstandings once this parameter is implemented in the models. This paper aims to clarify this issue. Moreover, the techniques found in literature aiming to measure this parameter are usually based on 2D approaches at low temperatures. In this paper, a 3D methodology to measure adiabatic self-heating is presented which considers all possible heat losses (conduction, convection, radiation and mass flux) through infrared measurements and Digital Image Correlation (DIC) technique. The adiabatic self-heating was measured for a widely used alloy (Ti6Al4V) obtaining promising results.

1. Introduction

Material characterization of metal alloys is commonly carried out through thermomechanical tests, for example, by using a Gleeble thermomechanical simulator, which allows high heating rates and accurate thermomechanical loading to be reached, the heating being controlled through Joule effect [1]. However, in practice, it is quite impossible to reach pure isothermal conditions due to heat conduction along the sample, conduction between anvils and sample and possible losses into the surroundings (convection and conduction) [2].

Bennet et al. [3] demonstrated that the stress measurements could differ more than 20% due to inhomogeneous temperature profile along the sample. This issue could lead to mispredictions on the material properties as stated by Evans and Scharning [4]. This thermal gradient could also influence the final microstructure [5]. Therefore, during thermomechanical characterization, a proper temperature control is essential. When the strain rate is low, usually lower than 0.001 s^{-1}, the process could be assumed to be isothermal as there is enough time to dissipate the heat. On the contrary, at higher strain rates, higher than 10 s^{-1}, the process can be assumed to be nearly adiabatic [6]. In the intermediate regime, the process is neither adiabatic nor isothermal [7,8].

Temperature is usually measured through thermocouples. For instance, Xiao et al. [2] carried out a comprehensive study to show the relevance of thermal gradients during material characterization. However, the thermal gradient was measured based on two thermocouples distributed along the sample, which could not reflect the thermal field properly. Similarly, Kardoulaki et al. [9] or Semiatin et al. [10] studied the effect of thermal gradients because of resistance heating by welding three thermocouples along the sample. Shao et al. [11] determined the heat flux along the sample during tensile testing with six thermocouples evenly distributed. This approach, although it could be more accurate, notably hampers the data treatment. Thermocouples, however, influence the heat flow acting as thermodynamic fins, they have limited tran-

* Corresponding author.
E-mail address: selabarrialandres@gmail.com (A. Sela).

https://doi.org/10.1016/j.ijheatmasstransfer.2022.123747

Nomenclature

β_1	adiabatic self-heating (definition 1)
β_2	adiabatic self-heating (definition 2)
W_p	energy introduced by the deformation process
F	compression load
L	displacement (compression test)
L_f	total displacement
Q_m	energy measured (infrared camera)
Q_{cond}	energy losses due to conduction
Q_{conv}	energy losses due to convection
Q_{rad}	energy losses due to radiation
Q_{mt}	energy losses due to mass fluxes
ρ	material density
c_p	specific heat capacity of the material
V	volume of the shear zone
ΔT_{IR}	temperature rise measured with the infrared camera
d_α	thermal diffusivity of the material
k	heat conduction
y_i	coordinate representing heat transfer
A_{loss}	section of losses
h	heat convection coefficient
T_{surf}	average temperature of the sample surface
T_{air}	temperature of the surroundings
ε_{em}	emissivity
σ_{SB}	Stefan–Boltzmann constant
RT	room temperature
DIC	digital image correlation
ROI	region of interest
IR	infrared radiation

sient response and they only allow single point measurements to be made [12,13]. In addition, the spatial resolution of thermocouples is limited, making them an unsuitable option when high thermal gradients are expected [14].

To address these issues, infrared cameras may be used to measure thermal fields. In comparison with thermocouples, this technique presents many advantages such as being a non-intrusive technique with a very fast response. However, the main disadvantage lies in the fact that sources of error such as emissivity, reflections, absorption and obstructions need to be controlled [15]. Van Rooyen et al. [14] proved that for a high-strain-temperature process this technique is more useful than thermocouples.

Together with a proper thermal control, it is worth mentioning that during plastic deformation the part being deformed is self-heated because of this high deformation (adiabatic self-heating phenomenon). The majority of the work employed in the deformation is transformed into heat while a small amount is kept as stored energy in lattice [6,8,16]. This temperature rise directly influences the test performance as it affects the flow curve of the material [17,18]. In addition, it may also affect the material microstructure, as stated by Feng et al. [19]. Therefore, the control and knowledge of this temperature rise is a key aspect on the performance of the thermomechanical characterization and to develop any accurate numerical model. Mirone and Barbagallo [20] stated that many material models neglect this adiabatic heating phenomenon.

Within this context, different definitions were found in literature which, in this work, have been distinguished as β_1 and β_2. The adiabatic self-heating, β_1, could be defined as it was previously done by Taylor and Quinney [21], as the ratio between the heat spent in heating the sample to the plastic work. This definition has been used for years and it is usually taken as 0.9–0.95 (or even 1) for many commercially available FEM software such as Deform, AdvantEdge or Forge NXT [8,22–24]. For instance, Mathieu et al. [25] and Cuesta et al. [26] included this coefficient in their thermal analysis of different manufacturing processes. In contrast, other researchers defined the adiabatic self-heating as the ratio between the heat experimentally observed via thermal variations to the total plastic work done [27–29], called as β_2 in this research. Under pure adiabatic conditions, these definitions would lead to the same result, however, when heat losses play an important role (at low strain rates or at high temperatures) the values reported could differ notably.

Table 1
Different values of adiabatic self-heating found in literature for Ti6Al4V under different conditions. Tests carried out at room temperature.

Strain rate (s^{-1})	Def.	β	Reference
460	β_2	0.2–0.7	[30]
3000	β_2	0.5–1.0	[31]
3000	β_2	0.4	[32]
2000	β_2	0.4–0.5	[28]
1500–3400	β_2	0.3–0.4	[28]
2800–7000	β_2	0.4–0.5	[28]
500–7000	β_2	0.5–0.6	[33]
0.001–0.01	β_1	0.6–0.9	[8]
1–50	β_1	0.9–0.98	[34]

However, in literature, both definitions are used indistinctly, which could lead to misunderstandings (see in Table 1 the variation of adiabatic self-heating parameter reported in literature for Ti6Al4V).

With regard to the measurement of the adiabatic self-heating, several attempts were found in literature aiming to measure it. Zhao et al. [35] measured it at 300 °C over a wide range of strain rates. In the study, heat losses due to radiation and convection were assumed to be negligible, which, even at 300 °C, could be a risky assumption leading to a bad estimation of the self-heating coefficient.

Rittel et al. [28] characterized the adiabatic self-heating for different materials, strain rates and load modes at room temperature. In spite of the comprehensive study carried out, heat losses such as conduction were not included in the analysis, which could explain the low values of adiabatic self-heating obtained at these elevated strain rates.

Bonk et al. [23] performed tensile tests in a vacuum chamber to avoid convection losses. A similar approach was taken by Knysh and Korkolis [8]. The temperature was measured with an infrared camera while Digital Image Correlation was used to determine possible heat losses due to mass flux. However, both approaches were carried out at low strain rates, typical from tensile tests but far different from industrial conditions and the problem was simplified as a 2D approach.

Also, the temperature is a relevant aspect to be taken into consideration when characterizing this coefficient [36,37] as higher temperatures may imply higher heat losses. Therefore, a proper way to characterize it at high temperatures is needed although it is briefly analysed in literature.

Thus, although adiabatic self-heating was experimentally measured by different researchers, no agreement was found between them as both definitions for adiabatic self-heating are used indistinctly reporting totally different results. In addition, the majority of the tests were made at low temperatures despite the relevance of temperature on heat losses.

This paper aims, therefore, to show a technique to measure the adiabatic self-heating for an aeronautical alloy (Ti6Al4V), considering heat losses by radiation, convection and conduction. The proposed technique considers a 3D control volume containing the re-

gion of interest according to DIC measurements aiming to enhance 2D techniques reported in literature. High speed infrared filming allows the evolution of the process to be determined and the adiabatic heating was obtained at different stages of the compression tests thanks to high speed infrared filming. The effect of temperature was also analysed within the paper.

The paper is organized as follows. The first section shows the physical background, employed methods, and used approximations to compute the adiabatic self-heating coefficient (heat losses, approaches). Then, the description of the experimental set-up is presented. To follow, the results are presented and discussed and, finally, the conclusions are shown.

2. Theoretical basis: heat transfer analysis

To carry out material characterization, the material is plastically deformed by controlling some physical parameters such as temperature, compression load and displacement, which define plastic strain and strain rate.

However, as stated above, due the to the energy conservation law, the sample temperature may change during the test. The amount of energy introduced by the deformation process, W_p, can be calculated by Eq. (1)

$$W_p = \int_0^{L_f} F dL \tag{1}$$

where F is the compression load and L is the displacement, that is, the area under the force curve obtained from the Gleeble tests.

According to the schematic view of the energy balance shown in Fig. 1, this energy is transformed as given by Eq. (2), including the expected proportion of each term.

$$W_p = Q_m + Q_{cond} + Q_{conv} + Q_{rad} + Q_{mt} + E_{stored} \tag{2}$$

The heat associated with the temperature rise measured with the infrared camera in the 3D control volume can be determined according to Eq. (3).

$$Q_m = \rho c_p V \Delta T_{IR} \tag{3}$$

where ρ and c_p are the density and the specific heat capacity of the material, assumed to be constant during the test, V is the volume of the shear zone (control volume) and ΔT_{IR} is the temperature rise measured with the infrared camera.

Following, Q_{cond} is referred to the heat transfer between the control volume and the rest of the sample by conduction (see Fig. 1). This heat loss can be quantified by Eq. (4) for an isotropic behaviour, which can be assumed for the small control volume chosen.

$$Q_{cond} = \rho c_p V d_\alpha \frac{\partial^2 T}{\partial y_i^2} = kV \frac{\partial^2 T}{\partial y_i^2} \tag{4}$$

where d_α is the thermal diffusivity of the material, T is the temperature, y_i represents the coordinate referred to the heat flux direction (vertical for this specific case) and k is the heat conduction. $\frac{\partial^2 T}{\partial y_i^2}$ was determined based on infrared measurements.

Then, convection losses to the surroundings can be calculated by Eq. (5).

$$Q_{conv} = A_{loss} h (T_{surf} - T_{air}) \tag{5}$$

where A_{loss} is the section of losses, this means the section in direct contact with the air, h is the heat convection coefficient of the air, which was set to 10 W/m^2 K according to Shitzer [38], T_{surf} is the average temperature of the sample measured with the infrared camera and T_{air} is the temperature of the surroundings (room temperature), both measured in K.

Likewise, the energy loss due to radiation to the surroundings is given by Eq. (6).

$$Q_{rad} = A_{loss} \varepsilon_{em} \sigma_{SB} (T_{surf}^4 - T_{air}^4) \tag{6}$$

where ε_{em} is the emissivity of the surface and σ_{SB} is the Stefan–Boltzmann constant.

Also, with the help of a high-speed filming camera and image correlation software it was shown that the heat loss related to mass fluxes was negligible in the present work.

Finally, E_{stored} is referred to other aspects such as restoration processes (dynamic recrystallization, recovery), the development of dislocation structures or stored lattice energy.

Therefore, the adiabatic self-heating can be calculated as:

$$\beta_1 = \frac{Q_m + (Q_{cond} + Q_{conv} + Q_{rad} + Q_{mt})}{W_p} \tag{7}$$

Alternatively, several authors, defined the adiabatic self-heating as the ratio between the heat measured via the temperature vari-

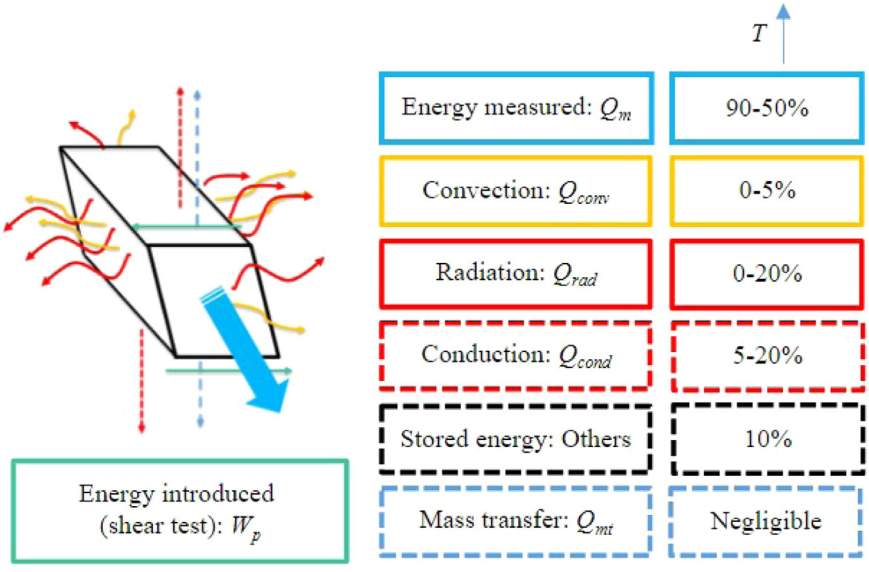

Fig. 1. Control volume considered for the adiabatic self-heating calculus.

ation and the plastic work, i.e.

$$\beta_2 = \frac{Q_m}{W_p} \tag{8}$$

3. Experimental set-up

Uniaxial compression loading of the specimens was carried out using a Gleeble 3500 thermomechanical testing machine. The specimens were located between two tungsten carbide anvils. The friction between the anvils and the specimen was negligible thanks to the use of graphite sheets. The vacuum chamber was opened so the process could be filmed. Therefore, vacuum was not created. This leads to heat losses due to convection and could cause the oxidation of the samples. Although oxidation could change the emissivity of the surface, this was constantly controlled through thermocouple measurement and IR camera comparison.

The machine heats the specimen based on the Joule effect with a heating rate of 10 °C/s up to the desired temperature. The testing temperature was held constant for 30 s to ensure the homogeneity along the sample. The temperature was controlled through a K-thermocouple welded to the specimen (see Fig. 2). In the present case, these temperatures were room temperature (RT) and 600 °C. The Gleeble machine records the force through a Kistler dynamometer and the displacement during the process, in order to analytically determine the plastic strain.

The specimen employed consisted of a shear sample similar to the one shown in Hor et al. [1]. The compressed distance was 2 mm and the speed was kept constant and set to 1.9 mm/s to keep the strain rate constant during the experimental test.

All the tests were filmed with a frame rate of 9000 frames per second using a Photron FASTCAM APX-RS250K. The objective used was a Navitar 12X. The sample was lit with HMI HSL 250 cool light (see Fig. 2(a)). Thanks to high speed filming, it was proven that the volume of the shear zone remained almost constant during the test, variations being lower than 5%, minimizing this source of error.

To carry out Digital Image Correlation (DIC) measurements from this surface, a speckle pattern was created. Different painting methods were tested to ensure good adhesion under the tested conditions, with enough resolution and no decorrelation problems. The aim of these measurements was to properly determine the shear zone and to obtain the strain fields. DIC analysis was done using GOM Correlate software. The noise error on plastic stain measurements was quantified by analysing the equivalent plastic strain obtained between 100 frames without movement, reporting plastic strain lower than 0.005.

Infrared images of the sample being deformed were taken using the FLIR Titanium 550 M with 1000 Hz of sampling frequency. The emissivity was characterized thanks to the thermocouple welded to the surface as Fig. 2(b) shows. At high temperatures, the effect of reflected temperature was totally negligible and the emissivity could be directly determined by comparing infrared and thermocouple measurements. However, at room temperature the effect of the reflected temperature must be properly characterized. In this case, the diffuser reflector method was employed [39]. The self-heating of the material was used as the heating source and the anvil reflection was employed to estimate the reflected temperature (see Fig. 3). For this specific case, the reflected temperature was 32 °C.

Finally, material microstructure was analysed so as to study the existence of some changes in the microstructure due to the deformation process. The deformed samples were mounted on resin and polished up to mirror finishing. Then, they were etched with Kroll's reagent to reveal the microstructure. For each sample geometry, the undeformed microstructure was compared with the deformed one at each temperature.

The material employed was the alloy Ti6Al4V, provided as a hot rolled bar with a diameter of 80 mm. The material was delivered in the annealed condition. Fig. 4 shows the microstructure with primary α grains and $\alpha + \beta$ colonies with an average grain size of 10.5 ASTM. The measured microhardness was $350HV_{0.05}$.

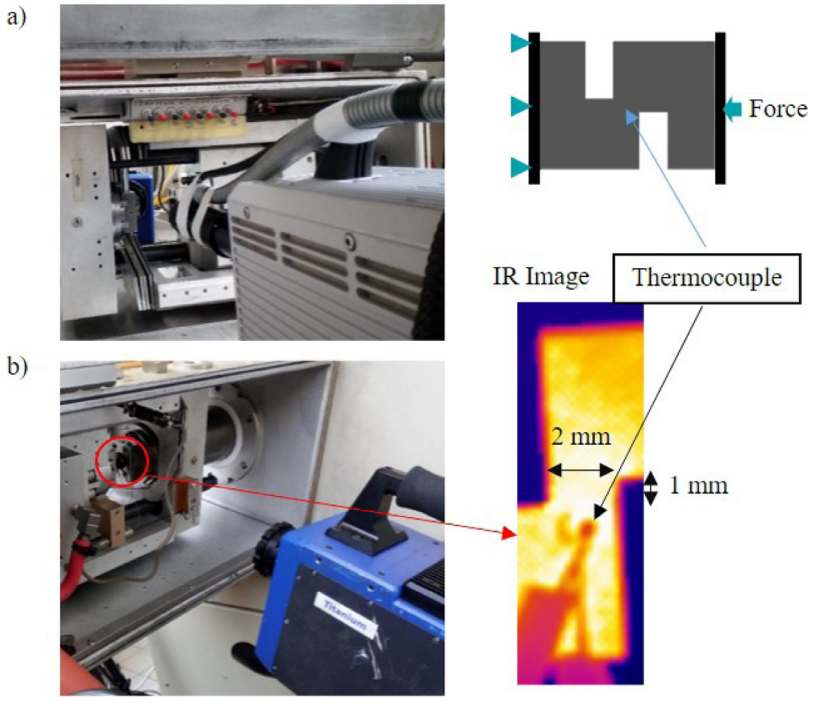

Fig. 2. Experimental set-up: a) Photron FASTCAM APX-RS250K with HMI HSL 250 cool light; b) FLIR Titanium 550 M with focus on the shear zone (infrared image) and the K-thermocouple.

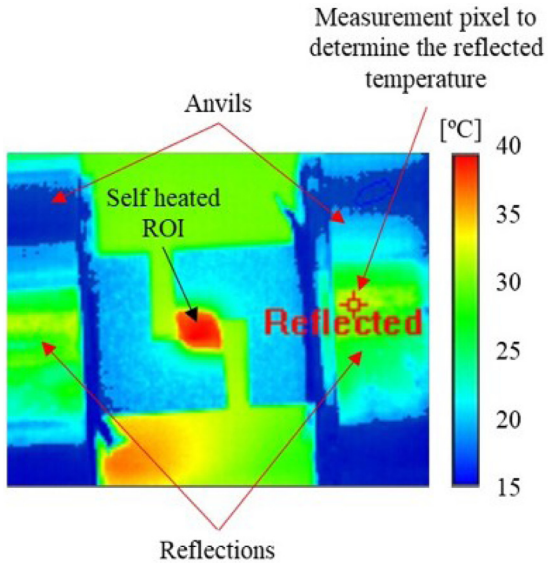

Fig. 3. Determination of the reflected temperature. Apparent temperatures given in Celsius degrees (ROI: Region of Interest).

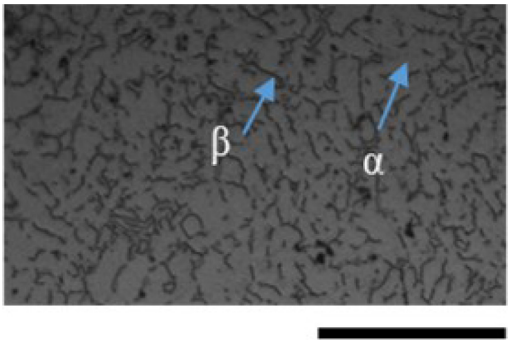

Fig. 4. Initial microstructure of the Ti6Al4V employed. Scale bar: 50 µm.

Table 2
Chemical composition of the Ti6Al4V.

Element	V	Al	Fe	C	O	N	Ti
Weight percent	4.05	6.36	0.16	0.015	0.019	0.006	Bal.

The density was 4430 kg/m^3 and the chemical composition is summarized in Table 2.

Material properties were taken from literature [40–42], the specific heat capacity being 519 and 680 J/kg K and the heat conductivity 6.7 and 10 W/mK, at room temperature and at 600 °C, respectively.

4. Results and discussion

4.1. Force analysis

The force results for each condition are shown in Fig. 5. The area within the curve represents the plastic work done (after removing the elastic effect). Two totally different behaviours were observed at the two temperatures. When the test was carried out at room temperature, the flow behaviour shows the typical strain hardening behaviour up to drastic brittle failure when the displacement was close to 1 mm.

In contrast, higher ductility was observed at 600 °C and no macroscopic failure seemed to take place. In addition, there is a decrease in the force when the displacement is close to 0.5 mm,

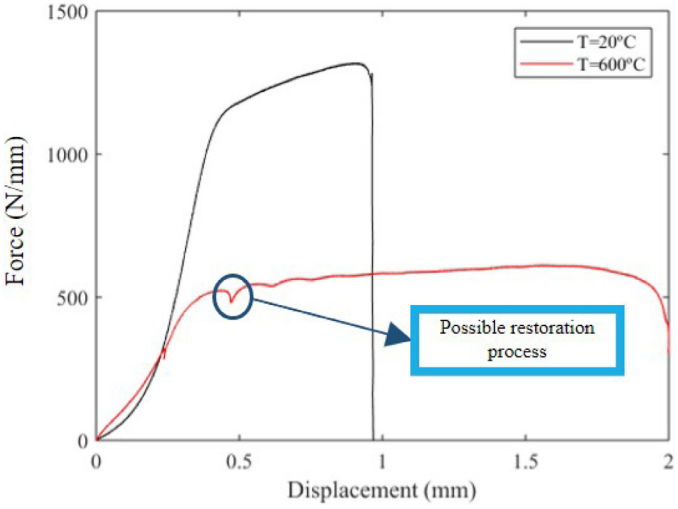

Fig. 5. Force-displacement diagrams (sample width = 10 mm).

which can be related to restoration microstructural processes such as dynamic recrystallization.

4.2. Digital image correlation analysis

The main aim of carrying out DIC analysis is to determine the volume of the shear zone in order to define the control volume and the area of losses so as to be applied in Eqs. (1)–(6). The relevance of the losses due to mass transfer was also analysed considering the speed component in *Y* direction.

The method employed was the widely accepted speckle painting technique due to its simplicity and cheapness. The test at 600 °C was taken as reference. The aim was to find a proper technique to obtain a surface with a good speckle pattern in order to measure strain at high temperatures. Therefore, the goal was to check the capability of the technique of being employed (in terms of adhesion, brightness or paint crack) rather than creating the best possible speckle pattern.

Eight different techniques were tested varying the surface finishing between polishing (etched and not), wire electro discharge machining (WEDM) surface and sandblasting. White speckles were randomly sprayed with Molydal NB 25 which consists of small particles of boron nitride. This paint works at temperatures up to 1000 °C. Some of the surfaces were previously painted black using two different types of paint, PYRO FEU matt black anti-caloric paint, resistant at high temperatures (up to 900 °C) and AREMCO HiE-Coat 840-MX ceramic-based, which is a black pigmented coating for metals up to 1300 °C.

Among all the techniques tested, at high temperature, the best technique found consisted of: (i) the WEDM surface was directly painted in black with AREMCO HiE-Coat 840-MX; (ii) the painting was cured to ensure good adhesion; (iii) white speckles were randomly spread along the surface with Molydal NB 25. For the tests at room temperature, the procedure was similar but the AREMCO black paint was substituted by PYRO-FEU 24950-6 900 °C thermal paint, making the curing process unnecessary at this temperature.

Measurements were carried out using GOM Correlate software. After determining the best option to create the speckle pattern, the quality was analysed using software criterion as it is shown in Fig. 6. The speckle sizes ranged from 0.02 to 0.12 mm. Because of the intense distortion expected (due to severe shear strain), the subset size was set to 60 pixels (which is 0.35 mm) with a step size of 20 pixels according to Society [43]. The subset size is the width of the square to mesh the reference image. The step size

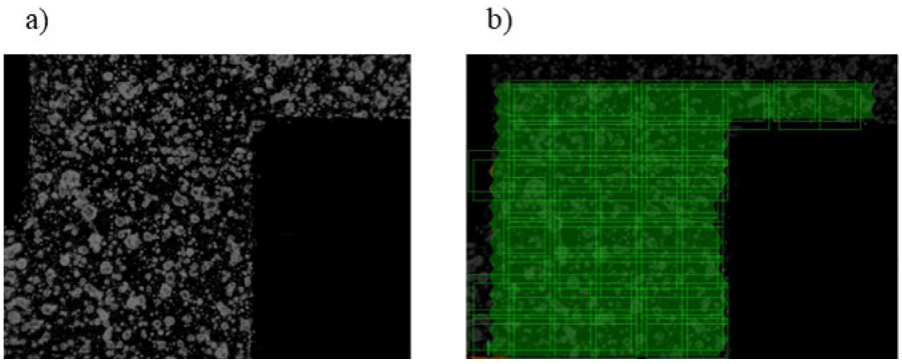

Fig. 6. a) Example of a speckle pattern employed for DIC analysis (at 600 °C). b) Quality of the speckle pattern created according to GOM Correlate software

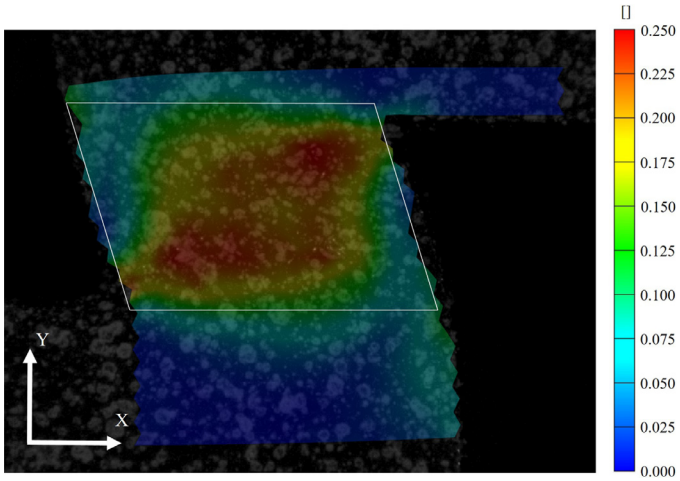

Fig. 7. Equivalent plastic strain field ($T = 600$ °C).

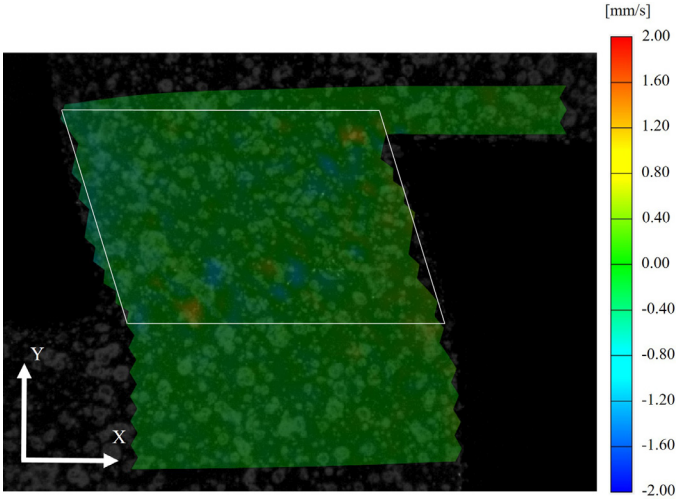

Fig. 8. Velocity in vertical direction: v_y field ($T = 600$ °C).

is the distance between subset centres. The noise error on plastic stain measurements was quantified analyzing the equivalent plastic strain obtained between 100 frames with the sample fixed between the anvils without movement. At both temperatures, the variation of plastic strain between these 100 frames was lower than 0.005.

As an example, a picture of the DIC measurements is shown in Fig. 7, the strain field obtained is similar to the ones shown in Bao and Wierzbicki [44], Leitao et al. [45] so the shear approach is assumed to be valid for the study. As can be seen, the shear zone can be approximated by a parallelepiped and its dimensions lead to a volume of 21 mm^3.

It is worth mentioning that the volume was observed to remain almost constant during deformation, once the shear zone had been formed, at both temperatures. The measured thickness of the shear zone, based on the equivalent strain field, was 1.38 mm.

The possible material fluxes into and out of the control volume may influence heat losses and could be relevant in the calculus of the adiabatic self-heating. Therefore, it is necessary to determine whether some particles tended to travel out of the control volume. To estimate it, the possible existence of velocity in Y direction would be a proper indicator. It is worth noting that compression forces were applied in horizontal direction according to Fig. 7. The velocity field in Y direction is shown in Fig. 8. At 600 °C no presence of velocity in Y direction was found. The same result was obtained at 20 °C. Thus, the heat losses due to mass transfer (Q_{mt}) were proved to be negligible.

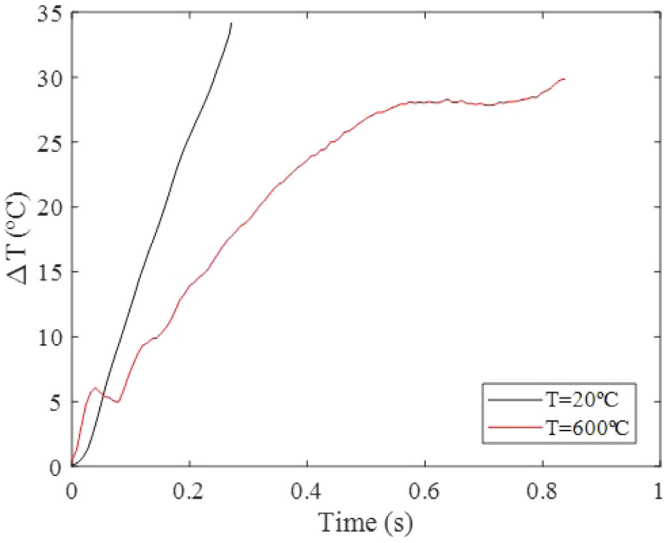

Fig. 9. Temperature rise during the process in the centre of the shear zone.

4.3. Surface temperature analysis

The temperature evolution of a point located in the centre of the shear zone was determined by tracking a 3×3 pixel. Fig. 9 shows the increment of the temperature with respect to the set one, that is, RT and 600°. It can be observed that the measured

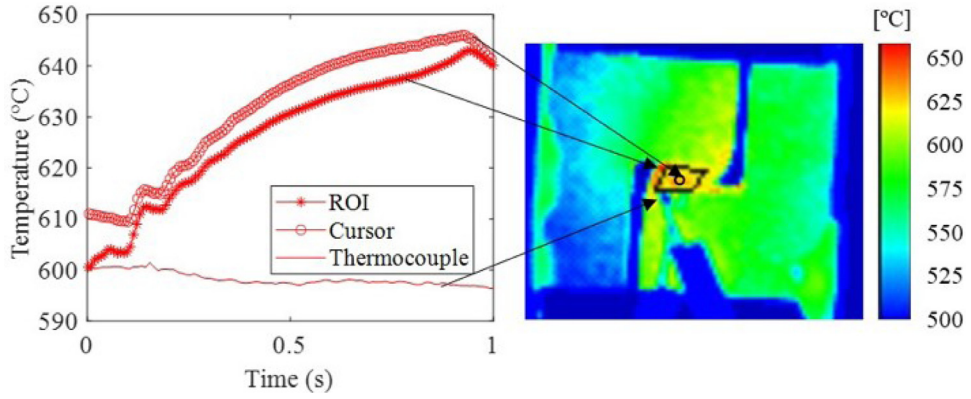

Fig. 10. Temperature evolution during a thermomechanical test (sample tested at 600 °C). $u_T = \pm 30$ °C.

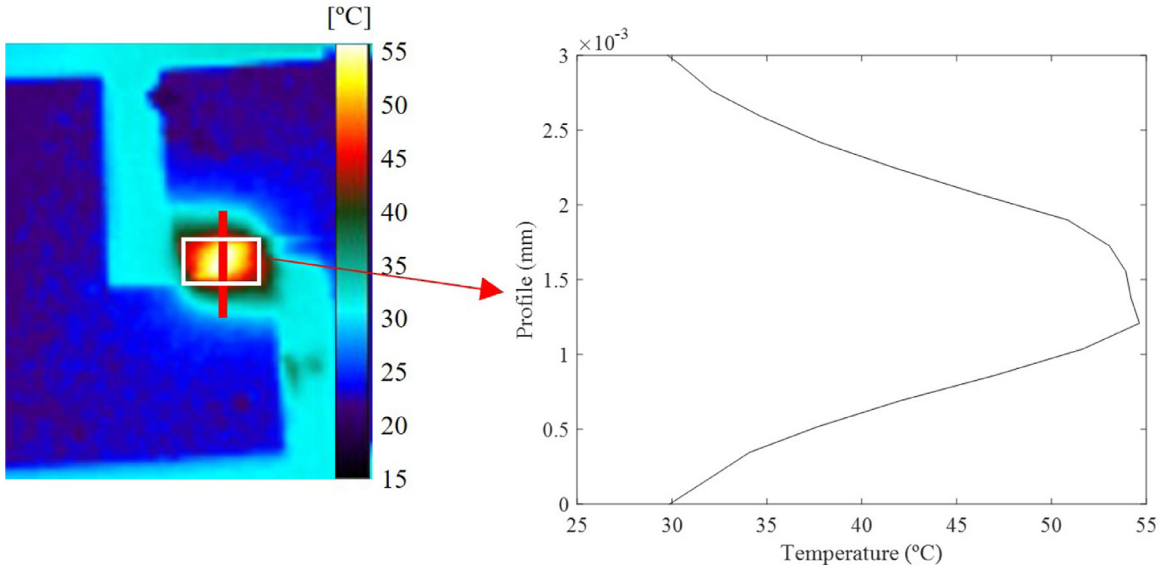

Fig. 11. Left: Temperature field within the shear zone at 20 °C. Right: Temperature profile along Y direction to determine heat losses due to conduction.

temperature increase was slightly higher in the room temperature case whereas the heating rate was notably higher.

To calculate heat losses due to convection (Q_{conv}) and radiation (Q_{rad}) the average temperature of the whole shear zone for each thermogram was used. For instance, in Fig. 10 the temperature evolution taking different measurement protocols can be seen, with no remarkable variation between the single point and the ROI measurement. However, it could be also observed that the use of thermocouples could lead to wrong values, as the measurement strongly depends on the position of the thermocouple, among other issues.

In order to also estimate the heat losses due to conduction it is necessary to determine $\frac{\partial^2 T}{\partial y_i^2}$. Based on infrared measurements, the conduction flux along the shear zone can be reduced to a flux in Y direction as Fig. 11 shows.

Based on Fig. 11 (right side), it can be seen that the temperature profile along the shear zone was symmetric. Therefore, in order to numerically calculate $\frac{\partial^2 T}{\partial x_i^2}$ (being $y_i = Y$ in the present case) the shear zone was divided into two halves. The average value of $\frac{d^2 T}{dY^2}$ was numerically calculated for each half at each frame. Finally, heat conduction losses can be estimated according to Eq. (4).

4.4. Determination of adiabatic self-heating

The results obtained at 20 °C are shown in Fig. 12. First of all, it is worth highlighting that radiation and convection losses were observed to be negligible under these conditions as they always represented less than 0.1 % of the whole energy. The term called as others in Fig. 12 represents the E_{stored}.

The average value of β_1 during the whole test was 0.88 which is in agreement with the values reported in literature [8]. In this case, the conduction losses progressively increase with time, reaching close to 5% of the total energy introduced. The value of β_2, calculated only considering Q_m and W_p was close to 0.84. With respect to the term "others", its value is around 10%, related to the stored energy in terms of microstructural aspects.

According to different authors, Ti6Al4V suffers flow instabilities and inhomogeneous flow at room temperature which may lead to adiabatic shear bands, resulting in local melting and fracture [46,47]. In Fig. 13 the initial and final microstructure at room temperature can be compared. In the final microstructure, a thin affected layer in which the microstructure is oriented in the fracture direction (probably an adiabatic shear band) can be seen, which could explain the stored energy.

The same analysis was carried out at 600 °C as Fig. 14 shows. Under this condition, radiation represents more than 20% of all of

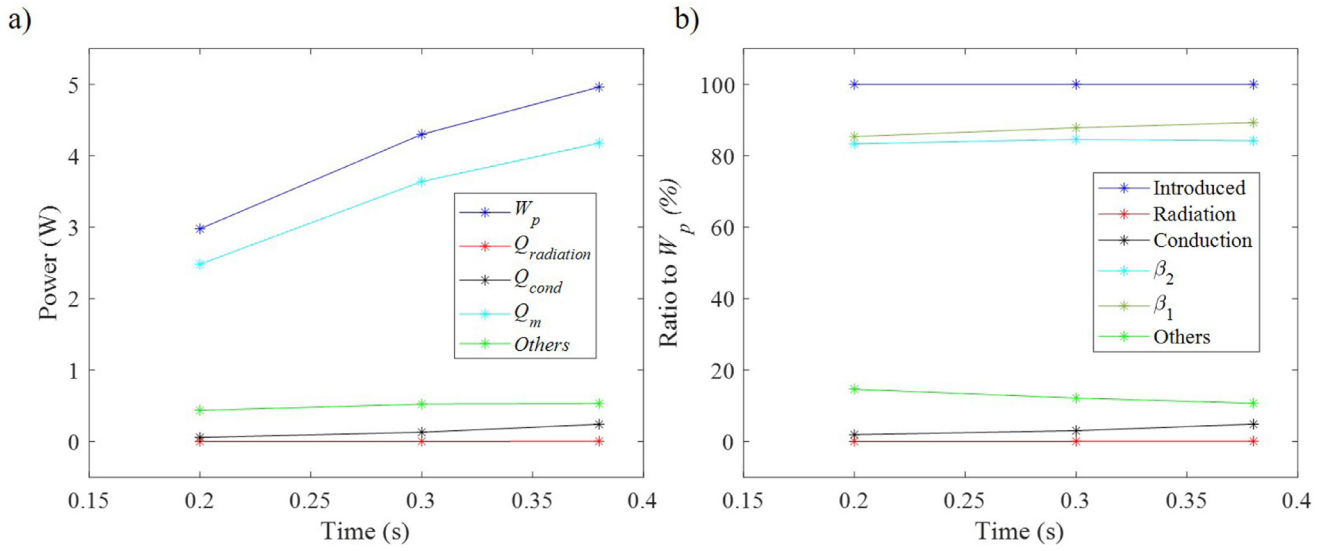

Fig. 12. Results at room temperature: a) Energy introduced and heat losses (in W), b) heat losses as a percentage of W_p to be directly related with Eqs. (7) and (8).

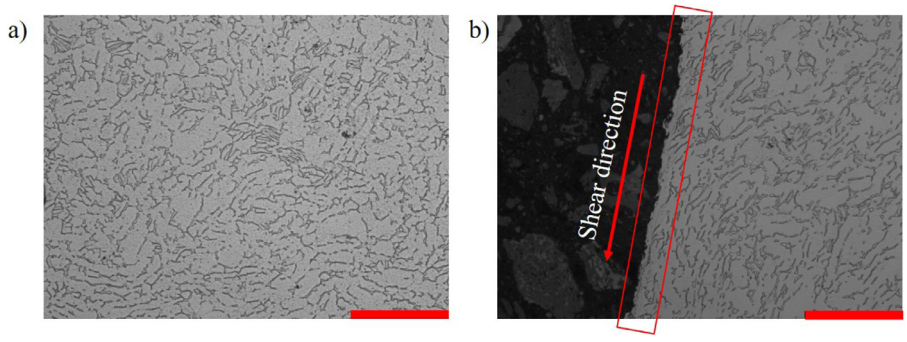

Fig. 13. Room temperature: a) Initial microstructure of Ti–6Al–4V ($\alpha + \beta$ structure), b) Microstructure after fracture: affected zone. Scale bar: 50 μm. Magnification: 500×.

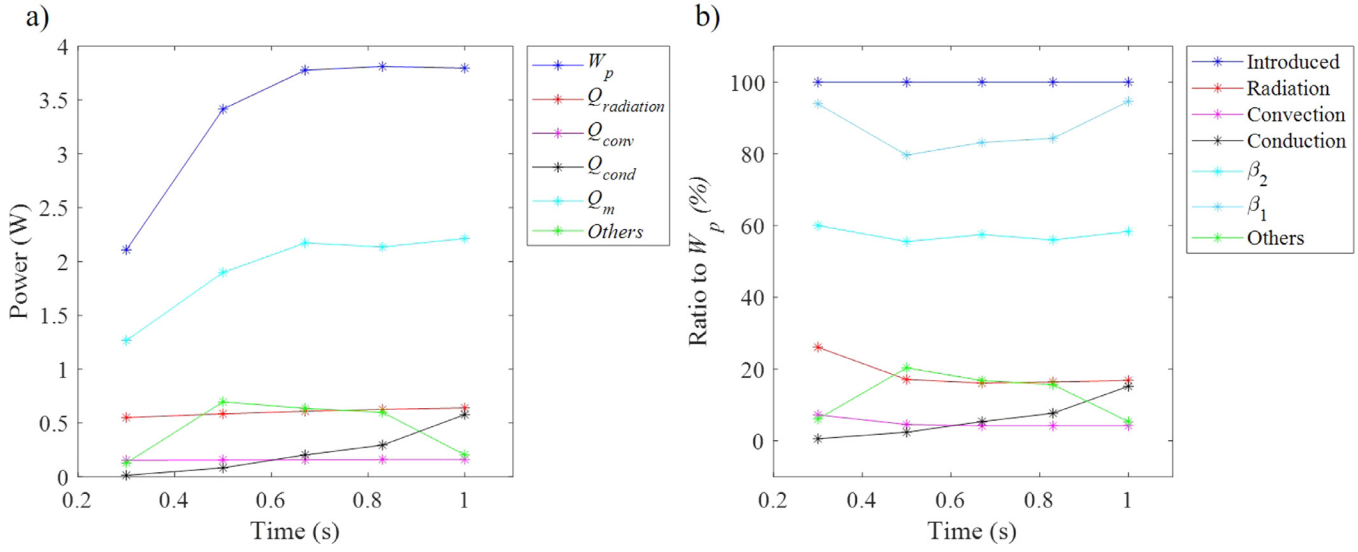

Fig. 14. Results at 600 °C: a) Energy introduced and heat losses (in W), b) heat losses as a percentage of W_p to be directly related with Eqs. (7) and (8).

the heat losses so this term has to be considered in the analysis to calculate the adiabatic self-heating coefficient. Convection losses could be also relevant, representing around 5% of the heat losses as a first approach.

The average value of β_1 was 0.87 again in agreement with the values reported in literature [8]. However, the value of β_2 was 0.57 due to thermal losses. Therefore, it can be seen that, when the heat losses are not relatively relevant (in the RT case radiation and convection losses were totally negligible), the values of β_1 and β_2 were quite close. These conditions are typical for tests carried out at high strain rates or at low temperatures. Finally, it is observed that the term “others”, again, represents around the 10% of all en-

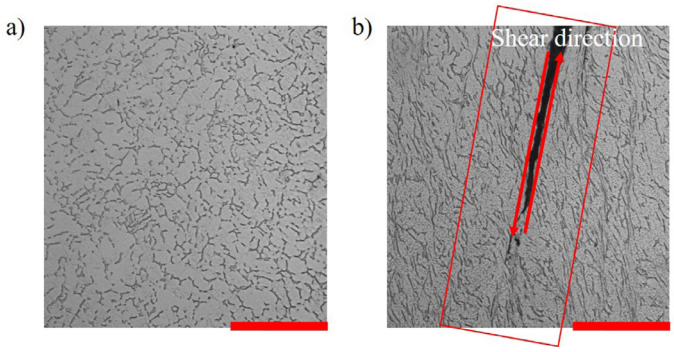

Fig. 15. T = 600 °C: a) Initial microstructure of Ti–6Al–4V ($\alpha + \beta$ structure), b) Microstructure after deformation: affected zone. Scale bar: 50 µm. Magnification: 500×.

ergy. As in previous case, under these conditions, adiabatic shear banding is expected [48].

The microstructure before and after the deformation test is shown in Fig. 15. As can be seen, the initial microstructure did not present any remarkable different compared with the one shown in Fig. 13a, so the heating up to 600 °C just increased the grain size. Although the crack has started, there has not been enough time to propagate and cause the drastic failure. In addition, grain elongation could be observed close to the shear banding zone, which could be an indicator of dynamic recovery, explaining the term others, as some authors reported [49,50].

The amount of energy stored was proved to be constant in the range of temperatures from 20 to 600 °C, the adiabatic heating coefficient (β_1) being close to the widely reported 90% under both conditions. As this parameter is important in numerical simulations, if the model is able to take into account thermal losses such as radiation or convection, its value can be assumed to be 0.9 whereas if the model does not include this, something typical for 2D models, its value should be corrected as radiation losses could represent more than 20% of all energy introduced in the system. In addition, this parameter is also relevant in material characterization as it determines the real temperature at which the test was carried out. It is worth mentioning that the sources of error were properly controlled during the experimental part: the volume of the shear zone was observed to remain almost constant; DIC measurement was proved to be accurate, reporting errors in the measurement lower than 0.005 for more than 100 frames at low and high temperature; the emissivity was controlled thanks to a continuous comparison between thermocouple measurement and IR values and the reflected temperature effect was taken into account for the RT case according to diffuser reflector method.

5. Conclusions

After analysing all the results, the following conclusions can be drawn:

- A novel 3D technique to measure the adiabatic self-heating under shear conditions is proposed considering heat losses and the energy measured through infrared measurement at different temperatures, demonstrating its capability at low and high temperatures.
- Adiabatic self-heating definitions found in the literature were clarified. The adiabatic heating, β_1, was demonstrated to be close to 0.9 as it is widely reported in literature under both conditions. This parameter is relevant on numerical simulations and can be set to 0.9 if the model is able to take into account heat losses such as convection or radiation.
- With this methodology, it was shown that, although β_1 remains almost constant at different temperatures, the value of β_2, due to the relevance of the heat losses, is notably lower when the temperature increases.

As further perspectives, the findings proposed in this paper provide new insights into material modelling as the methodology allows adiabatic self-heating to be characterized in order to be properly taken into account as it has been demonstrated that its value could be far from the widely used 0.9 due to thermal losses, improving the accuracy on numerical predictions.

Declaration of Competing Interest

The authors declare that they have no known competing financial interests or personal relationships that could have appeared to influence the work reported in this paper.

CRediT authorship contribution statement

A. Sela: Conceptualization, Formal analysis, Investigation, Methodology, Writing – original draft. **G. Ortiz-de-Zarate:** Investigation, Methodology, Resources. **D. Soler:** Formal analysis, Methodology, Software, Validation, Writing – original draft. **G. Germain:** Supervision, Writing – review & editing. **L. Gallegos:** Investigation, Methodology, Resources. **P.J. Arrazola:** Writing – review & editing, Supervision, Validation.

Data availability

Data will be made available on request.

Acknowledgements

The authors would like to thank the project SURFNANOCUT (RTI2018-095463-B-C21 and RTI2018-095463-B-C22) and the grant for Education and Training of Research Staff (FPU 17/02498).

References

[1] A. Hor, F. Morel, J.-L. Lebrun, G. Germain, An experimental investigation of the behaviour of steels over large temperature and strain rate ranges, Int. J. Mech. Sci. 67 (2013) 108–122.
[2] H. Xiao, X. Fan, M. Zhan, B. Liu, Z. Zhang, Flow stress correction for hot compression of titanium alloys considering temperature gradient induced heterogeneous deformation, J. Mater. Process. Technol. 288 (2021) 116868.
[3] C. Bennett, S. Leen, E. Williams, P. Shipway, T. Hyde, A critical analysis of plastic flow behaviour in axisymmetric isothermal and Gleeble compression testing, Comput. Mater. Sci 50 (1) (2010) 125–137.
[4] R. Evans, P. Scharning, Axisymmetric compression test and hot working properties of alloys, Mater. Sci. Technol. 17 (8) (2001) 995–1004.
[5] G.-Z. Quan, J. Pan, Z.-h. Zhang, Phase transformation and recrystallization kinetics in space–time domain during isothermal compressions for Ti–6Al–4V analyzed by multi-field and multi-scale coupling FEM, Mater. Des. 94 (2016) 523–535.
[6] L. Zhang, Thermo-mechanical characterization and dynamic failure of a CoCrFeNi high-entropy alloy, Mater. Sci. Eng. 844 (2022) 143166.
[7] M. Mataya, V. Sackschewsky, Effect of internal heating during hot compression on the stress-strain behavior of alloy 304 l, Metall. Mater. Trans. A 25 (12) (1994) 2737.
[8] P. Knysh, Y.P. Korkolis, Determination of the fraction of plastic work converted into heat in metals, Mech. Mater. 86 (2015) 71–80.
[9] E. Kardoulaki, J. Lin, D. Balint, D. Farrugia, Investigation of the effects of thermal gradients present in Gleeble high-temperature tensile tests on the strain state for free cutting steel, J. Strain Anal. Eng. Des. 49 (7) (2014) 521–532.
[10] S. Semiatin, D. Mahaffey, N. Levkulich, O. Senkov, The radial temperature gradient in the Gleeble® hot-torsion test and its effect on the interpretation of plastic-flow behavior, Metall. Mater. Trans. A 48 (11) (2017) 5357–5367.
[11] Z. Shao, N. Li, J. Lin, T.A. Dean, Strain measurement and error analysis in thermo-mechanical tensile tests of sheet metals for hot stamping applications, Proc. Inst. Mech. Eng., Part C 232 (11) (2018) 1994–2008.
[12] A. Hoyne, C. Nath, S. Kapoor, Cutting temperature measurement during titanium machining with an atomization–based cutting fluid (ACF) spray system, in: ASME 2013 International Mechanical Engineering Congress and Exposition, American Society of Mechanical Engineers, 2013, pp. 1–10.

[13] H.-J. Kröning, U. Lang, N. Hofmann, High temperature Gleeble microtensile testing of metallic micro specimens, Mater. Testing 58 (10) (2016) 826–832.
[14] M. van Rooyen, T.H. Becker, High-temperature tensile property measurements using digital image correlation over a non-uniform temperature field, J. Strain Anal. Eng. Des. 53 (3) (2018) 117–129.
[15] D. Soler, P. Aristimuño, A. Garay, P.J. Arrazola, Uncertainty of temperature measurements in dry orthogonal cutting of titanium alloys, Infrared Phys. Technol. 71 (2015) 208–216.
[16] A. Zubelewicz, Century-long Taylor–Quinney interpretation of plasticity-induced heating reexamined, Sci. Rep. 9 (1) (2019) 1–7.
[17] A. Chrysochoos, O. Maisonneuve, G. Martin, H. Caumon, J. Chezeaux, Plastic and dissipated work and stored energy, Nucl. Eng. Des. 114 (3) (1989) 323–333.
[18] L. Peroni, M. Scapin, Plastic behavior of laser-deposited Inconel 718 superalloy at high strain rate and temperature, Appl. Sci. 11 (16) (2021) 7765.
[19] F. Feng, S. Huang, Z. Meng, J. Hu, Y. Lei, M. Zhou, D. Wu, Z. Yang, Experimental study on tensile property of AZ31B magnesium alloy at different high strain rates and temperatures, Mater. Des. 57 (2014) 10–20.
[20] G. Mirone, R. Barbagallo, How sensitivity of metals to strain, strain rate and temperature affects necking onset and hardening in dynamic tests, Int. J. Mech. Sci. 195 (2021) 106249.
[21] G.I. Taylor, H. Quinney, The latent energy remaining in a metal after cold working, Proc. R. Soc. Lond. Ser. A 143 (849) (1934) 307–326.
[22] S. Dumoulin, H. Louche, O. Hopperstad, T. Børvik, Heat sources, energy storage and dissipation in high-strength steels: experiments and modelling, Eur. J. Mech. - A/Solids 29 (3) (2010) 461–474.
[23] C. Bonk, M. Vucetic, A. Bouguecha, B.A. Behrens, An experimental-numerical method to determine the plastic work converted into heat applied on AHSS, in: Advanced Materials Research, vol. 1140, Trans Tech Publ, 2016, pp. 51–58.
[24] G. Mirone, R. Barbagallo, M.M. Tedesco, D. De Caro, M. Ferrea, Extended stress-strain characterization of automotive steels at dynamic rates, Metals 12 (6) (2022) 960.
[25] G. Mathieu, V. Frederic, R. Vincent, F. Eric, 3D stationary simulation of a turning operation with an Eulerian approach, Appl. Therm. Eng. 76 (2015) 134–146.
[26] M. Cuesta, P. Aristimuño, A. Garay, P. Arrazola, Heat transferred to the workpiece based on temperature measurements by IR technique in dry and lubricated drilling of Inconel 718, Appl. Therm. Eng. 104 (2016) 309–318.
[27] Z. Pan, B. Sun, V.P. Shim, B. Gu, Transient heat generation and thermo-mechanical response of epoxy resin under adiabatic impact compressions, Int. J. Heat Mass Transf. 95 (2016) 874–889.
[28] D. Rittel, L. Zhang, S. Osovski, The dependence of the Taylor–Quinney coefficient on the dynamic loading mode, J. Mech. Phys. Solids 107 (2017) 96–114.
[29] S. Härtel, M. Graf, B. Awiszus, K.G. Abstoss, R. Hild, Novel approach for the determination of the Taylor–Quinney coefficient, in: Materials Science Forum, vol. 918, Trans Tech Publ, 2018, pp. 103–109.
[30] D. Macdougall, J. Harding, The measurement of specimen surface temperature in high-speed tension and torsion tests, Int. J. Impact Eng. 21 (6) (1998) 473–488.
[31] J. Mason, A. Rosakis, G. Ravichandran, On the strain and strain rate dependence of the fraction of plastic work converted to heat: an experimental study using high speed infrared detectors and the Kolsky bar, Mech. Mater. 17 (2–3) (1994) 135–145.
[32] D. Rittel, Z. Wang, Thermo-mechanical aspects of adiabatic shear failure of AM50 and Ti6Al4V alloys, in: Engineering Systems Design and Analysis, vol. 48357, 2008, pp. 529–550.
[33] J.L. Smith, J.D. Seidt, A. Gilat, Full-field determination of the Taylor–Quinney coefficient in tension tests of Ti–6Al–4V at strain rates up to 7000 s^{-1}, in: Advancement of Optical Methods & Digital Image Correlation in Experimental Mechanics, vol. 3, Springer, 2019, pp. 133–139.
[34] S. Bruschi, S. Poggio, F. Quadrini, M. Tata, Workability of Ti–6Al–4V alloy at high temperatures and strain rates, Mater. Lett. 58 (27–28) (2004) 3622–3629.
[35] D. Zhao, Temperature correction in compression tests, J. Mater. Process. Technol. 36 (4) (1993) 467–471.
[36] S. Oh, S. Semiatin, J. Jonas, An analysis of the isothermal hot compression test, Metall. Trans. A 23 (3) (1992) 963–975.
[37] R. Goetz, S. Semiatin, The adiabatic correction factor for deformation heating during the uniaxial compression test, J. Mater. Eng. Perform. 10 (6) (2001) 710–717.
[38] A. Shitzer, Wind-chill-equivalent temperatures: regarding the impact due to the variability of the environmental convective heat transfer coefficient, Int. J. Biometeorol. 50 (4) (2006) 224–232.
[39] R. Usamentiaga, P. Venegas, J. Guerediaga, L. Vega, J. Molleda, F.G. Bulnes, Infrared thermography for temperature measurement and non-destructive testing, Sensors 14 (7) (2014) 12305–12348.
[40] J.J. Li, W.L. Johnson, W.-K. Rhim, Thermal expansion of liquid Ti–6Al–4V measured by electrostatic levitation, Appl. Phys. Lett. 89 (11) (2006) 111913.
[41] M. Boivineau, C. Cagran, D. Doytier, V. Eyraud, M.-H. Nadal, B. Wilthan, G. Pottlacher, Thermophysical properties of solid and liquid Ti–6Al–4V (TA6V) alloy, Int. J. Thermophys. 27 (2) (2006) 507–529.
[42] N. Milošević, I. Aleksić, Thermophysical properties of solid phase Ti–6Al–4V alloy over a wide temperature range, Int. J. Mater. Res. 103 (6) (2012) 707–714.
[43] I.D.I.C. Society, A good practices guide for digital image correlation, 2018,
[44] Y. Bao, T. Wierzbicki, On fracture locus in the equivalent strain and stress triaxiality space, Int. J. Mech. Sci. 46 (1) (2004) 81–98.
[45] C. Leitao, M. Costa, K. Khanijomdi, D. Rodrigues, Assessing strength and local plastic behaviour of welds by shear testing, Mater. Des. 51 (2013) 968–974.
[46] S.V. Kailas, Y. Prasad, S. Biswas, Flow instabilities and fracture in Ti–6Al–4V deformed in compression at 298 K to 673 K, Metall. Mater. Trans. A 25 (10) (1994) 2173–2179.
[47] Y.-M. Luo, J.-X. Liu, X.-W. Cheng, S.-K. Li, F.-C. Wang, W.-W. Guo, Adiabatic shear banding of hot-rolling Ti–6Al–4V alloy subjected to dynamic shearing and uniaxial dynamic compression, Rare Met. 34 (9) (2015) 632–637.
[48] N. Reddy, Y.-H. Lee, J.H. Kim, C.S. Lee, High temperature deformation behavior of Ti–6Al–4V alloy with and equiaxed microstructure: a neural networks analysis, Met. Mater. Int. 14 (2) (2008) 213.
[49] S. Roy, S. Suwas, The influence of temperature and strain rate on the deformation response and microstructural evolution during hot compression of a titanium alloy Ti–6Al–4V–0.1B, J. Alloys Compd. 548 (2013) 110–125.
[50] L. Mosecker, A. Göttmann, A. Saeed-Akbari, W. Bleck, M. Bambach, G. Hirt, Deformation mechanisms of ti6al4v sheet material during the incremental sheet forming with laser heating, in: Key Engineering Materials, vol. 549, Trans Tech Publ, 2013, pp. 372–380.